ISIJ International, Vol. 33 (1993), No. 2, pp. 313–320

Texture and Microstructure of Ti–49at%Al after Dynamic Recrystallization and Annealing

Christian HARTIG, Hiroshi FUKUTOMI,[1)] Heinrich MECKING and Kiichi AOKI[1)]

Technical University Hamburg, Harburg, Eissendorfer Street, 2100 Hamburg, 90 Germany.
[1)]Yokohama National University, Tokiwadai, Hodogaya-ku, Yokohama, Kanagawa-ken, 240 Japan.

(*Received on July 20, 1992; accepted in final form on October 16, 1992*)

A Ti–49at%Al gamma-base titanium alloy was deformed at high temperature ($T=1\,150$–$1\,200$°C) and low strain rates as well as at lower temperature ($T=1\,000$°C) and higher strain rates. Textures with distinctly different strength occurred depending on the deformation conditions. Subsequent heat treatments were applied in order to investigate the development of textures and microstructures. Textures and microstructures after deformation at $1\,150°C<T<1\,200°C$ are stabilized by α_2-Ti_3Al-precipitates at the γ-TiAl grain boundaries which occur after the first annealing at 1 050°C.

KEY WORDS: TiAl; compression; recrystallization; texture; precipitation.

1. Introduction

In the last few years the ductility and fracture toughness of alloys based on the intermetallic compound γ-TiAl have been improved by a combination of several techniques such as alloying of ternary elements,[1,2)] thermomechanical treatments[3)] and production of directionally solidified 2-phase α_2-Ti_3Al/γ-TiAl alloys.[4)] At high temperature deformation the occurrence of dynamic recrystallization (hereafter abbreviated DRX) has been found,[5,6)] which offers the possibility to control the microstructure under conditions of a better workability of TiAl. Some mechanisms of texture formation during DRX have been proposed,[6,7)] however, the role of the deformation and recrystallization in the texture evolution is not known in detail. More information about texture evolution during deformation as well as dynamic and static recrystallization and also about its relationship with microstructure development is needed. To this end, compression textures after DRX and the texture development during subsequent annealing were investigated in the present study.

2. Experimental

2.1. Preparation of Specimens and Compression Tests at High Temperatures

Testing material was produced from pure Ti and Al by Ar arc melting in a water cooled copper crucible. The result of a chemical analysis was as follows: 48.7at% Al, 0.047wt% Fe, 0.123wt% O, 0.011wt% N. For the compression tests, four specimens were cut having a size of 9 mm in diameter and a height of 10 mm. They were homogenized under vacuum at 1 200°C for 24 h. For compression testing a hydraulic machine specially designed for low strain rates was utilized. The compression tests were carried out in vacuum at high temperature ($T=1\,150$–$1\,200$°C) and low strain rates as well as at lower temperature ($T=1\,000$°C) and higher strain rates (**Table 1**) up to a maximum true strain of $\varepsilon=-1.8$. After testing the specimens were furnace cooled to room temperature within 3 h.

2.2 Annealing Treatments, Texture Measurements, Metallography and ECP-measurements

Before annealing layers of 0.6 mm of the upper side and 0.4 mm of the lower side of the specimens were removed in order to avoid the influence on recrystallization and texture of specimen regions deformed non uniaxially. For the deformed state and for each state of the subsequent annealing treatments the texture and the microstructure of the upper side of the specimens were

Table 1. Deformation conditions and annealing steps of specimens 1–4.

Treatment	Spec. 1	Spec. 2	Spec. 3	Spec. 4
Deformation temperature [°C]	1 200	1 150	1 000	1 000
Strain rate [s^{-1}]	10^{-4}	10^{-4}	2×10^{-4}	10^{-3}
Peak stress [MPa]	57	77	253	308
State after the				
1st anneal	1 050°C, 1 h			
2nd anneal	1 050°C, 2 h			
3rd anneal	1 050°C, 4 h			
4th anneal	1 050°C, 4 h + 1 200°C, 0.5 h			
5th anneal	1 050°C, 4 h + 1 200°C, 3.5 h			
6th anneal	1 050°C, 4 h + 1 200°C, 12.5 h			

examined. The annealing treatments were conducted under vacuum at two different temperatures in 6 steps (Table 1). Before each examination a specimen layer of 50 μm was removed together with the oxidated surface. It is well known that vacuum annealing of TiAl often causes severe Al vaporization resulting in a Ti-rich surface layer. Therefore after the last examination further 120 μm were removed from specimen 1 for a check of a possible difference in microstructure between the areas 50 and 170 μm below the surface.

Pole figure measurements in γ-TiAl exhibit some experimental problems due to the weak tetragonality ($c/a=1.02$) resulting in an overlap of the Bragg reflections *hkl* and *lkh*. Since the appropriate way of texture determination for this case is described elsewhere,[9] only a short outline will be given here. In this study texture measurements were carried out in the following way: {201) and {111)* pole figures were measured with a narrow receiving slit for a better signal to background ratio and for a better separation from the α_2-reflections. The measurements of {002)/{200) and {220)/{022) overlapping pole figures were carried out using a broad receiving slit in order to obtain a complete superposition of the overlapping reflections. The back reflection method was implemented in the "circular scan" mode with a maximum tilt angle of 75°. Using an extension of the harmonics method of quantitative texture analysis[17] a texture analysis was carried out incorporating the pole figures containing superpositions of crystal directions *hkl* and *hlk*.

For metallography the specimens were polished after each annealing step and the microstructure was examined by optical microscopy using polarized light.

For the determination of single orientations and the correlation with their location in the microstructure the specimens were examined in a scanning electron microscope using diffraction by electron channeling. Imaging and diffraction contrast could be considerably improved by electrolytic ethching.

3. Results

3.1. Microstructure

The microstructure of the cast and annealed material before deformation exhibited large grains (diameter 100–500 μm) of irregular shape. The volume fraction of the α_2-phase was in the range of a few percent **(Fig. 1(a))**.

After high temperature deformation two different types of microstructure developed depending on the deformation conditions. In the case of deformation at high temperatures and low strain rates (hereafter abbreviated as HTLS) the specimens contained large grains of equiaxed shape (Fig. 1(b)). After deformation at moderate temperatures and higher strain rates (hereafter abbreviated as MTHS) the microstructure consisted of two fractions: a coarse-grained fraction of agglomerated large grains and a fine-grained fraction

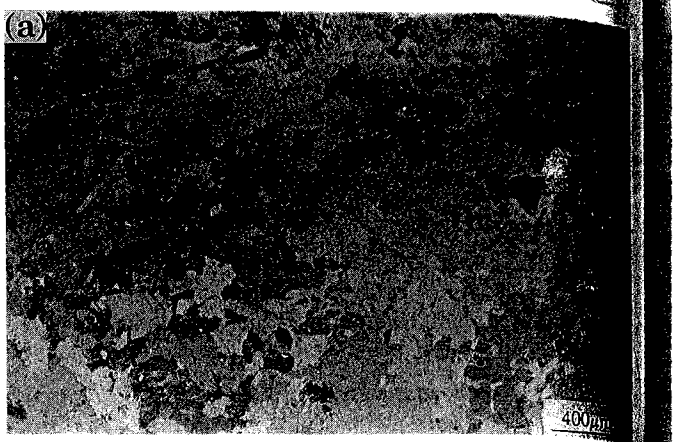

Fig. 1(a). Microstructure of Ti–49at%Al in the as cast and annealed state. (polarized light)

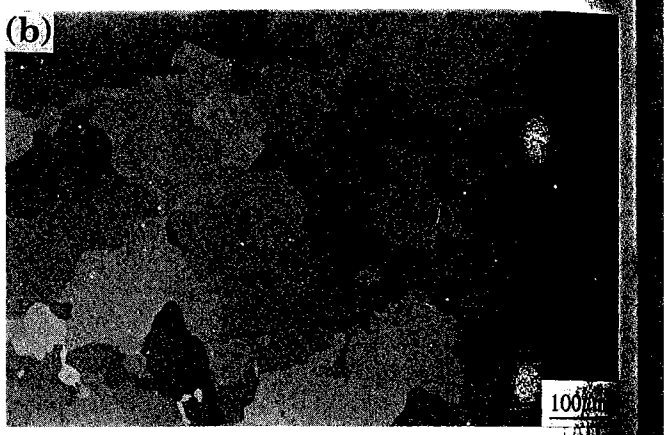

Fig. 1(b). Microstructure of specimen 2 (HTLS case) after deformation (polarized light) shown in compression direction.

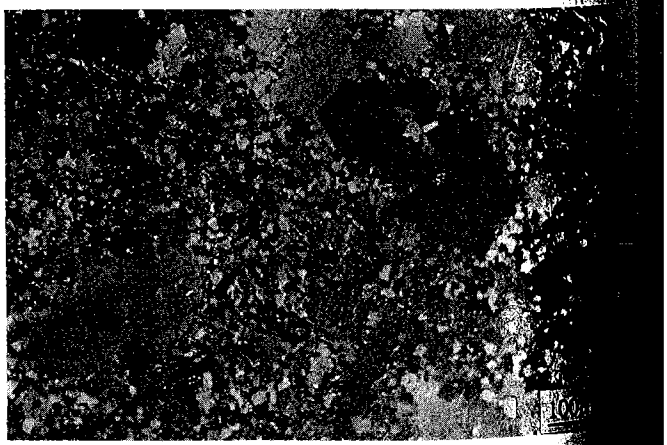

Fig. 2. Microstructure of specimen 3 (MTHS case) after deformation. (polarized light)

filling the volume between the coarse-grained **(Fig. 2)**.

The α_2-Ti_3Al phase disappeared in the HTLS specimens during deformation.

After the first annealing (1 h at 1 050°C) a visible change of the microstructure occurred

* Because of the tetragonal crystal structure the following notations are used: {*hkl*) for common planes and ⟨*uvw*] for common directions. *l* and *w* must not be interchanged with *h*, *k* or *u*, *v* respectively.

MTHS case specimens: inside the coarse grains small grains developed and in the fine-grained areas homogeneous grain growth took place (**Fig. 4(a)**). The arithmetic mean value of the grain size did not change drastically (**Fig. 3**). In the HTLS specimens the grain size became somewhat smaller during the first annealing (Fig. 3). By scanning electron microscopy the precipitation of a second Ti-rich phase at the grain boundaries of the HTLS case specimen 1 was detected (Fig. 4(b)). A more detailed determination of this phase was not been carried out, but according to general experience it can be assumed to be α_2-Ti_3Al.

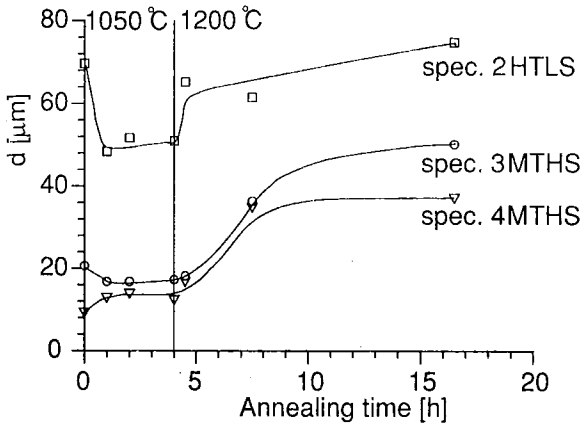

Fig. 3. Grain sizes (arithmetic mean values from line cutting method of specimens 2, 3, 4) as function of the annealing time.

Fig. 4(a). Microstructure of specimen 3 (MTHS case) after the first annealing.

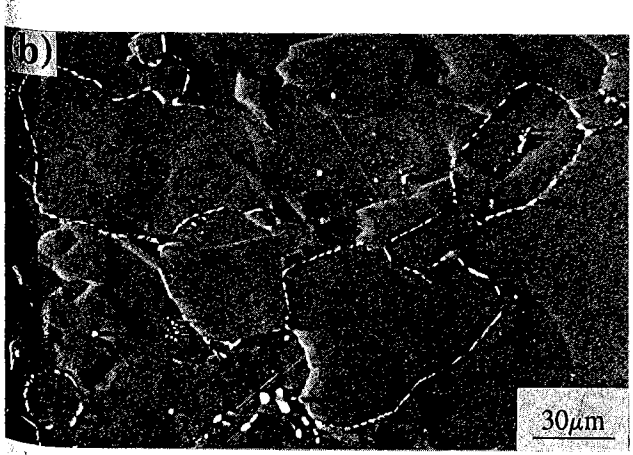

Fig. 4(b). SEM-micrograph of specimen 1 (HTLS case) after the first annealing.

By the next two annealing treatments at 1 050°C the microstructure in all specimens did not change and the precipitation of α_2-Ti_3Al at the grain boundaries of both HTLS case specimens became more clearly visible by SEM. In the case of MTHS specimens, precipitation could also be detected by SEM.

The precipitates lead to a stabilization of the grain size at 1 050°C. For a more relevant test of stability of the microstructure with respect to grain size and texture the annealing temperature of the next annealing steps was changed to 1 200°C.

The annealing treatments at 1 200°C changed the microstructure obviously in the MTHS case resulting in a homogeneous spatial distribution of the grain sizes by distinctive grain growth (Fig. 3). In the HTLS case the grain size changed visibly during the first annealing step at 1 200°C and moderately during the remaining annealing treatments (Fig. 3). The α_2-Ti_3Al phase continued to precipitate not only at the grain boundaries but also in the interior of γ-TiAl grains (**Fig. 5**). In the case of specimen 1 almost no change of the microstructure between the areas 50 and 170 μm below the surface was observed after the last annealing treatment indicating that effects of diffusion of Al to the surface could be neglected.

In all frequency distributions of the measured grain sizes the statistical scatter (calculated as the standard deviation of a Gaussian normal distribution) had almost the same magnitude and showed the same trend as the mean grain size itself. This is considered to be caused by the statistics and geometry of growth but in this paper this will not be followed up in more detail.

3.2. Texture

The {111}-pole figure of cast and annealed Ti–49at%Al before deformation shows peaks of individual grains originating from large TiAl grains (**Fig. 6**). The orientations seem to be not perfectly randomly distributed indicating a very weak texture. After deformation the texture of the γ-TiAl phase was analyzed from 4 pole figures (cf. Sec. 2.2). The texture will be represented here by the inverse pole figures of the compression direction. The inverse pole figures of the radial direc-

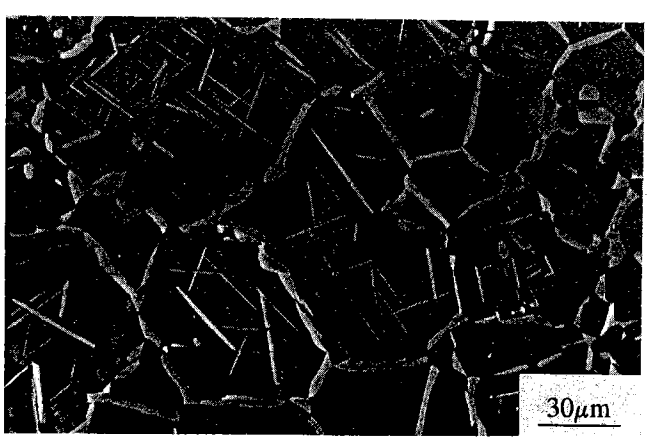

Fig. 5. SEM-micrograph of specimen 1 (HTLS case) after the sixth annealing.

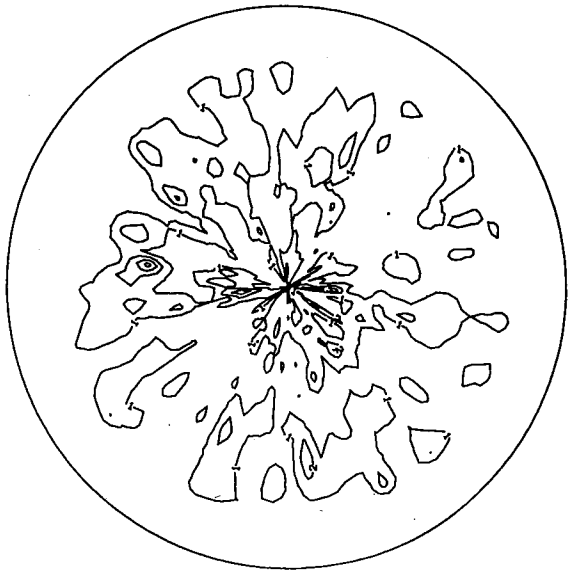

Fig. 6. {111}-pole figure of TiAl-alloy in the as cast and annealed condition. Levels are multiples of a random pole density.

tions show a practically uniform random distribution of crystal orientations for all the measured textures and therefore they can be omitted here. Thus the inverse pole figures presented give a complete description of the distribution of the specimen axes (*i.e.* the compression direction) in the frame of the tetragonal crystal lattice. After deformation the texture was quite different from the texture prior to deformation for all 4 specimens (**Fig. 7**): the two HTLS case specimens after deformation have a quite pronounced texture revealing a single, strong maximum of the distribution of the compression axes in the vicinity of {302} (less than 1° distance). For the two MTHS case specimens the texture was somewhat different: in both specimens the texture was quite weak with one moderate maximum at {712} in specimen 4 whereas in specimen 3 one somewhat greater maximum was found almost exactly at {302}.

After one annealing step at 1 050°C minor texture changes in the MTHS case specimens occurred: in specimen 3 the maximum at {302} weakened and shifted to {11,0,3} in the inverse pole figure (**Fig. 8a**)). A maximum at the same position {11,0,3} occurred in specimen 4 (**Fig. 8c**)). By further annealing at 1 050 and

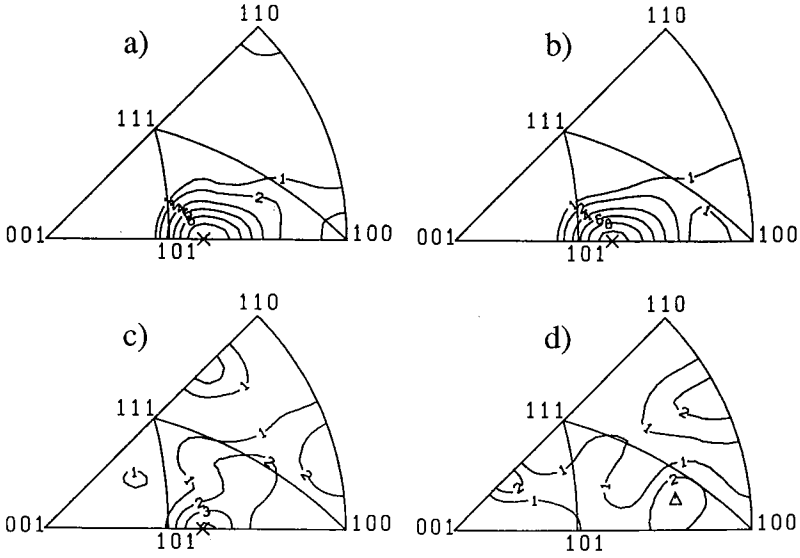

Fig. 7.
Inverse pole figures of specimens 1–4 after deformation at elevated temperatures as given in Table 1. Levels are multiples of a random orientation density: a) spec. 1, b) spec. 2, c) spec. 3, d) spec. 4. × – {302}, △ – {712}

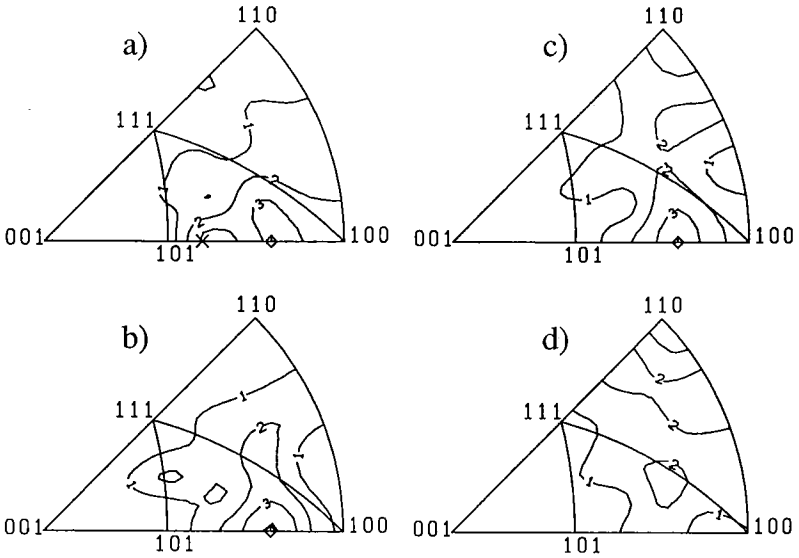

Fig. 8.
Inverse pole figures of specimens 3 and 4 after first and sixth annealing treatment: a) spec. 3, first annealing, b) spec. 3, sixth annealing, c) spec. 4, first annealing, d) spec. 4, sixth annealing, × – {302}, ◇ – {11,0,3}

1 200°C this maximum vanished in specimen 4 (**Fig. 8b**)) whereas in specimen 3 it became somewhat sharpened (Fig. 8b)).

In the HTLS case specimens the large maximum at {302) changed only slightly by annealing. The volume fraction of orientations within a distance of 15 degrees from this maximum decreased slightly for both specimens after the first annealing steps at 1 050°C and increased again during the last annealing step at 1 200°C (**Fig. 9a**)). The volume fraction of orientations for an area with a 5°-radius, which is very sensitive to the maximum height, did not change during annealing (**Fig. 9b**)). From this it follows that annealing affects primarily the local frequency distribution in the vicinity of the maximum rather than the maximum value itself. According to Fig. 9 the global change of the {302) component does not exceed 15% in both specimens and is correlated with a change in volume fraction of two other side maxima at {001) and at {338) which increase during the decrease of the {302) component and *vice versa* as shown for the case of specimen 2 (**Fig. 10**).

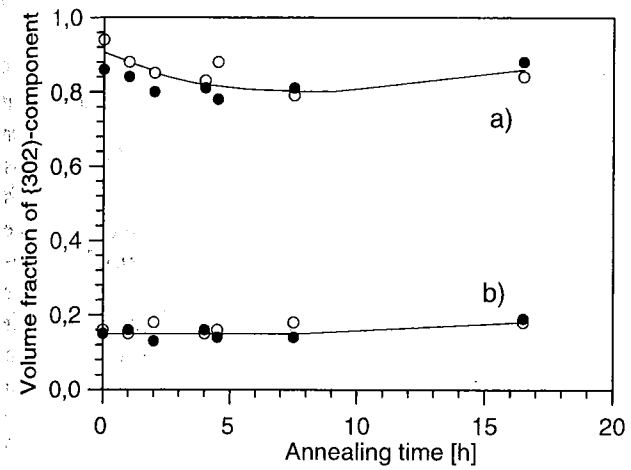

Fig. 9. Volume fraction of the {302)-component in specimens 1 (○) and 2 (●) calculated by an angular criterion: a) 15° difference from {302), b) 5° difference from {302).

3.3. Orientation Determination of Individual Grains by Electron Channeling Patterns (ECP)

A more detailed evaluation of the ECP measurements of single orientations has yet to be completed. From the ECP-method applied to specimens 1 and 2 the following preliminary results can be stated:

(1) The orientations of single grains are in agreement with the orientation distribution as shown in the inverse pole figures.

(2) Orientations in the vicinity of the maximum {302) belong to somewhat larger grains than other orientations far from {302).

4. Discussion

4.1. Texture and Microstructure after Dynamic Recrystallization

In the present work the change of textures as well as the evolution of microstructure after previous deformation of TiAl at high temperatures has been strongly influenced by the precipitation of α_2-Ti_3Al. Only the deformed specimens after DRX did not exhibit any precipitation. First the formation of the textures in the

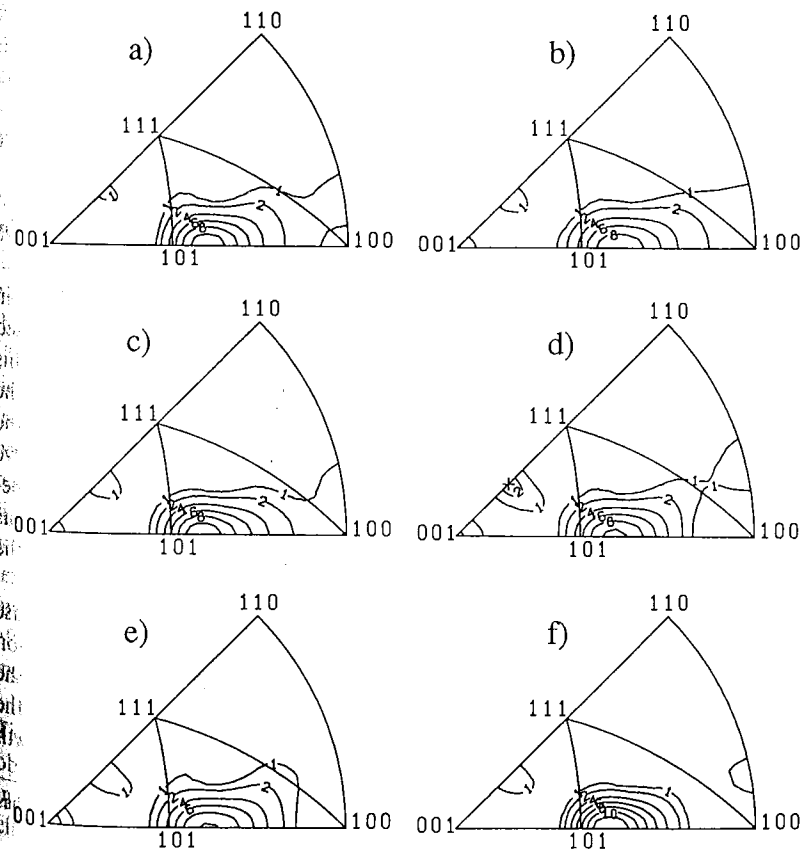

Fig. 10.
Inverse pole figures of specimen 2. Advancing annealing treatments in the sequence a–f (*e.g.* a) ≡ after first annealing treatment *etc.*, + – {338)).

deformed states including the usual aspects of texture formation under the absence of phase transformations will be discussed.

The deformation textures as well as the recrystallization textures of γ-TiAl have been studied by a few groups until now.[6-9] After deformation at low temperatures (450°C) a texture with the main component {110} and a weaker component {101), the latter being somewhat shifted towards {100), has been found.[9] This texture can be considered as a pure deformation texture because no recrystallization was found.

From another investigation about texture formation by dynamic recrystallization it could be concluded that under low peak stress conditions a fibre texture with the main component {101} evolves thereby becoming sharper with a decrease in peak stress.[7] Until now a decision about the exact crystallographic type of this component (whether {110}- or {101)-type) and its shape in the orientation space was not possible. In the present investigation this component has been confirmed as the {302)-component described in Sec. 2.2. It can be considered to be consistent with the results of previous measurements[6,7] which show a strong maximum in the center of the {202) pole figures. Bulging and continuous rotation of grains without the nucleation of new grains was given as the predominant mechanism for the formation of this type of DRX-texture.[7] Thus the texture is interpreted to be primarily a deformation texture in which some components are possibly missing since during bulging a certain fraction of grains might be "eaten up" by growing grains but new ones can not be created. This explanation is supported by deformation textures measured at low temperatures (T=450°C) not being influenced by DRX. Also there a maximum of the pole density was found in the vicinity of the {302) position.[9]

However, it has to be pointed out that the {110) component being observed after deformation at lower temperatures is completely missing after DRX under conditions of high temperatures and low strain rates (cf. Figs. 7 and 10). This implicates two possible explanations: (1) The glide mechanisms (*i.e.* glide modes, twinning) and the correspondent texture at high temperatures are different from those at low temperatures. (2) The {110) component is "eaten up" during recrystallization (*i.e.* by preferential growth of the {302)-component at the expense of {110)). The first explanation seems to be not very likely because texture simulation (based on Taylor's theory of polycrystal deformation) including effects of the anisotropy of the critical resolved shear stresses for ⟨110] and ⟨101] slip never resulted in a disappearance of the {110) component.[8] Also the incorporation of other physical aspects of deformation ("invalidity" of Schmid's law, twinning) does not seem to cause a total disappearance of this component. Hence the more probable explanation is that the {302)-component grows at the expense of the {110)-component during DRX. Such growth capability is due to a difference in driving forces which may be caused by differences in surface energy (*i.e.* an advantage in size) or by differences in volume energy (*i.e.* dislocation density) of the {302) grains. Also the different mobility of grain boundaries may have an influence on growth statistics and thus on texture evolution. For a difference in surface energy some evidence is found in the results of the ECP-measurements, indicating an advantage of the {302)-component in size. A difference in volume energy caused by dislocation density may arise by a stronger deformation (*i.e.* crystallographic shear Γ) of the {110)-oriented grains. From the relation between crystallographic shear and macroscopic strain (ε):

$$d\Gamma = d\varepsilon \cdot M \qquad (M\text{: Taylor factor})$$

being also valid in a modified form in the case of anisotropic flow stress,* it follows that under the Taylor-type of polycrystal deformation (ε=const.) the Taylor factor M must be larger for {110) than for {101) in this case. This holds only if the critical resolved shear stress for ⟨101] superdislocation glide is larger than the critical resolved shear stress for ⟨110] normal dislocation glide.[9] Although this relation between the shear stresses is in accordance with present conceptions it seems to be unlikely that it is valid also at very high temperatures when all obstacles to dislocation motion can be overcome easily by thermal activation. Hence the growth capability of the {302)-component is more likely to be caused by a size advantage.

After DRX at low temperature (MTHS case) the grain size is much smaller than at high temperatures (low peak stress conditions) and the texture is randomized. Hence it is concluded that microstructure and texture occuring under high peak stress conditions are controlled by the nucleation of new grains as has already been pointed out.[7] The occurrence of the weak {302)-component in specimen 3 can be ascribed to a lower peak stress in comparison to specimen 4 where this component does not occur.

4.2. Development of Texture and Microstructure by Annealing

After deformation no α_2-phase could be detected in the HTLS case specimens. However, α_2 precipitated during annealing also at deformation temperature. This result cannot be easily explained on the basis of the presently known phase diagrams[15,16] and probably the influence of the pressure produced during compressive deformation is important for the transformation behaviour near the $\gamma/\gamma+\alpha_2$ transus line. We leave this as a suggestion for further experimental work about the pressure dependence of the Ti–Al phase diagram.

The microstructure of the annealed HTLS case specimens is decisively controlled by the precipitation of Ti_3Al. This follows from the observation of the microstructure which exhibits Ti_3Al precipitates at the grain boundaries of the γ-TiAl phase. The grain growth

* The total amount of crystallographic shear Γ expressed as the sum of individual crystallographic shears has to be somewhat modified. This has no influence on the validity of this equation.

occurring under the annealing treatments at 1 200°C only in the first step can be compared with a law of grain growth (*i.e.* the $t^{1/2}$-law of Beck[10]) which is known for single phase materials.

During the second and third annealing step at 1 200°C only very sluggish grain growth takes place which is not consistent with any of the laws of grain growth for single phase materials described in the literature.[10,11] The textures also exhibit no drastic but only moderate or small changes during annealing. Thus it can be stated that the precipitates effectively suppress nucleation and large scale grain boundary migration, leading to recrystallization *in situ* (or continuous recrystallization). In spite of it some minor changes in microstructure and texture occur:

(1) There exists a tendency of the main {302}-component of the HTLS case specimens to become weaker during the first steps of annealing and to sharpen again in the final annealing treatment.

(2) During the first annealing treatment at 1 050°C the grain size decreased and increased again during the annealing steps at 1 200°C.

(3) Along with the main {302}-component some minor components ({001} and {338}) occur with growth dynamics opposite to those of the main component.

These results indicate the presence of some nucleation during the first annealing steps in connection with the development of minor texture components. Although more than 90 vol% of the material belong to a single, main fibre component, the formation of the minority components could be partially caused by the nucleation of new grains stimulated by the annihilation of dislocations. Under the assumption that the main component exhibits preferred growth, a sharpening of this component during the final annealing steps can be explained. There exists some experimental evidence for this assumption. However, it needs further experimental confirmation by orientation measurements of individual grains.

The absence of components of texture such as for example {100}, {833} and {203} leads to the conclusion that the tetragonality of the lattice strongly influences the evolution of texture during annealing. A comparison with annealing textures of cubic metals may therefore be misleading. Nevertheless in the case of the {338}-component a similarity may exist with conventional fcc-metals. In fcc-metals a {114}-component (neighbouring {338}) is observed experimentally and predicted by texture simulations including effects of relaxed constraints after deformation under compression conditions.[12] The recrystallization texture observed here may be related to this type of deformation texture but a further discussion requires more experimental investigation of the recrystallization textures after compression of TiAl as well as of conventional fcc metals.

In the MTHS case specimens the precipitation of Ti_3Al at the grain boundaries of γ-TiAl was not so obvious as for the HTLS case specimens. Thus changes in texture and microstructure are not suppressed so efficiently as in the HTLS case specimens and the recrystallization becomes more discontinuous.

A different evolution of annealing texture was observed for specimens 3 and 4, respectively: in the case of specimen 4 a component {11,0,3) arises after the first annealing treatment disappearing again during the following annealing treatments whereas in specimen 3 the same component increases by annealing. This difference may be due to a difference in driving force for the nucleation of new grains (*i.e.* dislocation density) being somewhat larger in the case of specimen 4 which was deformed at higher stresses. In accordance with a previous work[7] it can be assumed that in specimen 4 the nucleation of grains leading to a randomization of the texture may be more pronounced than in specimen 3. Specimen 3, however, was deformed at somewhat lower stresses and exhibits a minor {302)-component after deformation. This component is consumed by the {11,0,3)-component. Because of the lower level of nucleation in this specimen the resulting growth advantage by the increase in size of the {11,0,3)-oriented grains can become sufficient for a predominance of this component in the final annealing treatments at 1 200°C.

The recrystallization behaviour for the MTHS case specimens is somewhat different from that often observed in supersaturated solid solutions: In a variety of commercial alloys (Al–Cu, Ni–Al, Ni–Cr–Al *etc.*) it has been found that a discontinuous precipitation during recrystallization always leads to a random texture because growth selection is suppressed owing to impurity drag by segregation of solutes at grain boundaries.[13] On the other hand, it has also been observed that in Cu–Ag alloys precipitation does not substantially change the recrystallization mechanisms but only the recrystallization kinetics.[14] Thus the interaction between recrystallization and precipitation has to be considered to be slightly different depending on the segregating element and the alloying system as well as on time and temperature.[14] The behaviour of specimen 4 becoming randomized in texture by annealing is in accordance with the observation by Hornbogen and Kreye[13] but the behaviour of specimen 3 is not. Hence an explanation based on neglecting of segregation effects seems to give a better description. For a more detailed investigation of the interaction between recrystallization and precipitation (including also effects resulting from the different kinetics[14] of these two contributions) in the case of γ-TiAl-alloys further experimental work especially about the formation of recrystallization textures is necessary.

5. Conclusions

This paper gives a first survey of the types of textures in a γ-TiAl alloy after annealing of dynamically recrystallized specimens. The following results and conclusions could be obtained:

(1) The type of texture developing after DRX under high stress peak conditions and low peak stress conditions are quite different. Specimens deformed under low peak stress conditions exhibit an intense single component {302)-fibre texture whereas specimens de-

formed under high peak stress conditions show a more random texture with minor {302}- and {11,0,3}-components.

(2) The development of texture and microstructure of Ti–49at%Al in the more coarse grained specimens deformed under low stress peak conditions is drastically influenced by the presence of Ti_3Al-precipitates. That results in a recrystallization behaviour similar to recrystallization *in situ*.

(3) In the more fine grained specimens deformed under high stress peak conditions the texture becomes random or somewhat more pronounced depending on the peak stress and the texture after DRX. A {11,0,3}-component becomes more intense by annealing.

The result of a recrystallization *in situ* with a stabilization of the microstructure of the γ-TiAl phase by the presence of Ti_3Al-precipitates may be of major importance for the further development of γ-TiAl alloys for structural applications. It offers the possibility of a retainment of the texture and microstructure together with a decrease of the dislocation density, which is required in forming processes and high temperature thermal treatments.

Acknowledgments

The authors are grateful to T. Kamijo, T. Sakai (University of Electro-Communications, Tokyo) for valuable discussions and to T. Takatori (Nippon Mining Company Ltd.), H. Sugiuchi and I. Todo for generously making available the TiAl-alloy and the technical equipment necessary for this investigation. Thanks are also due to M. Dahms (GKSS-GmbH, Geesthacht) for support with programs for the ODF-calculation. One of the authors (Ch.H.) was sponsored by the JSPS (Japan Society for the Promotion of Sciences).

REFERENCES

1) T. Tsujimoto and K. Hashimoto: High-Temperature Ordered Intermetallic Alloys III, Vol. 133, ed. by C. T. Liu, A. I. Taub, N. S. Stoloff and C. C. Koch, MRS, (1989), 391.
2) Young-Won (Y.-W.) Kim: Proc. Int. Symp. Intermetallic Compounds—Structure and Mechanical Properties—(JIMIS6), ed. by O. Izumi, The Jpn. Inst. Metals, Sendai, (1991), 753.
3) J. Seeger, Ch. Hartig, A. Bartels and H. Mecking: High-Temperature Ordered Intermetallic Alloys IV, Vol. 133, ed. by C. T. Liu, A. I. Taub, N. S. Stoloff and C. C. Koch, MRS, (1991), 157.
4) M. Takeyama, T. Hirano and T. Tsujimoto: Proc. Int. Symp. Intermetallic Compound—Structure and Mechanical Properties—(JIMIS6), ed. by O. Izumi, The Jpn. Inst. Metals, Sendai, (1991), 507.
5) Ch. Hartig, S. Chen, P. A. Beaven and H. Fukutomi: 6th World Conference on Titanium, Part II, ed. by P. Lacombe, R. Tricot and G. Beranger, Les Editions de Physique, Paris, (1989), 1021.
6) H. Fukutomi, Ch. Hartig and H. Mecking: *Z. Metallkd.*, **81** (1990), 272.
7) H. Fukutomi, S. Takagi, K. Aoki, H. Mecking and T. Kamijo: Proc. Int. Symp. Intermetallic Compounds—Structure and Mechanical Properties—(JIMIS6), ed. by O. Izumi, The Jpn, Inst. Metals, Sendai, (1991), 839.
8) S. R. Nishitani, M. H. Oh, A. Nakamura, T. Fujiwara and M. Yamaguchi: *J. Mater. Res.*, **5**, (1990), No. 3, 484.
9) Ch. Hartig, X.-F. Fang, H. Mecking and M. Dahms: *Acta Metall. Mater.*, **40** (1992), 1883.
10) P. A. Beck: *Adv. Phys.*, **3** (1954), 245.
11) G. Abbruzzese and K. Lücke: *Acta Metall.*, **34** (1986), 905.
12) M. G. Stout, J. S. Kallend, U. F. Kocks, M. A. Przystupa and A. D. Rollett: VIIIth Int. Conf. Textures of Materials (ICOTOM8), ed. by J. S. Kallend and G. Gottstein, The Metall. Soc., (1988), 479.
13) E. Hornbogen and H. Kreye: Texturen in Forschung und Praxis, J. Grewen, G. Wassermann, Springer Verlag, Berlin, (1969), 274.
14) W. Kim and G. Gottstein: VIIIth Int. Conf. Textures of Materials (ICOTOM8), ed. by J. S. Kallend and G. Gottstein, The Metall. Soc., (1988), 649.
15) E. L. Hall and S. C. Huang: *Acta Metall. Mater.*, **38** (1990), 539.
16) J. C. Mishurda and J. H. Perepezko: Personal communication, (1991).
17) M. Dahms and H. J. Bunge: Theoretical Methods of Texture Analysis, DGM-Informationsgesellschaft, Oberursel, (1987), 143.